HHS Public Access

Author manuscript

Acta Biomater. Author manuscript; available in PMC 2019 September 01.

Published in final edited form as:

Acta Biomater. 2018 September 01; 77: 85–95. doi:10.1016/j.actbio.2018.07.032.

Mechanical Confinement via a PEG/Collagen Interpenetrating Network Inhibits Behavior Characteristic of Malignant Cells in the Triple Negative Breast Cancer Cell Line MDA.MB.231

Daniel S. Reynolds[1], **Kristen M. Bougher**[1], **Justin H. Letendre**[1], **Stephen F. Fitzgerald**[2], **Undina O. Gisladottir**[1,3], **Mark W. Grinstaff**[1,4,5], and **Muhammad H. Zaman**[1,6,*]

[1]Department of Biomedical Engineering, Boston University, Boston, MA, 02215, USA.

[2]Department of Biomedical Engineering, Rensselaer Polytechnic Institute (RPI), Rensselaer, NY, 12180, USA.

[3]Department of Biomedical Informatics, Harvard Medical School, Boston, MA, 02215, USA.

[4]Department of Chemistry, Boston University, Boston, MA, 02215, USA.

[5]Department of Medicine, Boston University School of Medicine, Boston, MA, 02118, USA.

[6]Howard Hughes Medical Institute, Boston University, Boston, MA, 02215

Abstract

To decouple the effects of collagen fiber density and network mechanics on cancer cell behavior, we describe a highly tunable *in vitro* 3D interpenetrating network (IPN) consisting of a primary fibrillar collagen network reinforced by a secondary visible light-mediated thiol-ene polyethylene glycol) (PEG) network. This PEG/Collagen IPN platform is cytocompatible, inherently bioactive via native cellular adhesion sites, and mechanically tunable over several orders of magnitude—mimicking both healthy and cancerous breast tissue. Furthermore, we use the PEG/Collagen IPN platform to investigate the effect of mechanical confinement on cancer cell behavior as it is hypothesized that cells within tumors that have yet to invade into the surrounding tissue experience mechanical confinement. We find that mechanical confinement via the IPN impairs behavior characteristic of malignant cells (i.e., viability, proliferation, and cellular motility) in the triple negative breast cancer cell line MDA.MB.231, and is more effective than removal of soluble growth signals. The PEG/Collagen IPN platform is a useful tool for studying mechanotransductive signaling pathways and motivates further investigation into the role of mechanical confinement in cancer progression.

[*]Corresponding author: Muhammad H. Zaman, Ph.D., Address: 44 Cummington St. Boston, MA 02215, Tel: (617) 358-5881, Fax: (617)353-6766, zaman@bu.edu.

Contributions

Conceived and designed the experiments: D.S.R., M.W.G., and M.H.Z. Performed the experiments: D.S.R., K.M.B., J.H.L., S.G.F., and U.O.G. Analyzed the data: D.S.R., K.M.B., J.H.L., S.G.F, and U.O.G. Wrote the manuscript: D.S.R., M.W.G., and M.H.Z. All authors reviewed and commented on the manuscript.

Graphical Abstract

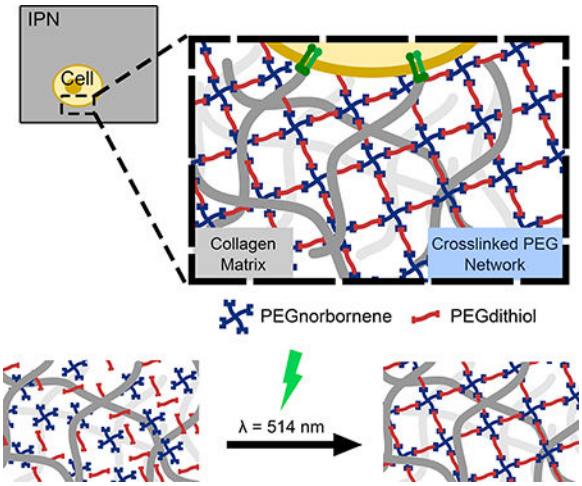

Keywords

Interpenetrating network; thiol-ene “click” chemistry; 3D *in vitro* tumor model; cancer mechanobiology

1. Introduction

The tumor microenvironment is characterized by a stiffened extracellular matrix (ECM) often displaying enhanced collagen deposition, crosslinking, and fiber alignment[l,2]. Furthermore, this abnormal microenvironment actively contributes to cancer progression by promoting the invasion of the basement membrane, uncontrolled proliferation, and loss of apicobasal polarity[1,3,4]. However, the exact biophysical mechanisms underlying this behavior remain unclear. Therefore, to better understand how the tumor microenvironment contributes to cancer progression, recent studies are moving beyond the study of purely biochemical mechanisms and investigating the contributions and role of ECM physical properties such as stiffness[l,2], pore size[5], and viscoelasticity[4,6].

The physical properties of the ECM are sensed by cells via a process known as mechanotransduction[7]. Traditionally, mechanotransduction is investigated using two-dimensional systems, such as polyacrylamide gels, which offer the capacity to investigate individual parameters independently: for example, the effects of substrate stiffness are differentiated from ligand composition and density[8–12]. However, many of the elements integral to mechanotransduction in 2D (e.g., focal adhesions, stress fibers, and lamellipodia) are diminished or entirely absent within cells cultured in 3D environments[13–17]. Therefore, a need exists to probe the effects of the physical microenvironment on cancer cell behavior within 3D cell culture systems, which better recapitulates the 3D *in vivo* tumor microenvironment than 2D systems. But in 3D cell culture systems, the physical parameters of stiffness, ligand composition, and ligand density become more entangled and are difficult to decouple. Despite this, a significant effort is ongoing to define them with studies

involving synthetic biomaterials[18,19], naturally-derived biomaterials[1,2], and combinations of the two[20,21].

For purely synthetic polymeric biomaterials, cells are typically encapsulated within hydrogels[22,23]. Such an approach has the advantage of being highly tunable, often with elastic moduli spanning several orders of magnitude, but suffers from a lack of natural cell-adhesion sites and an inability to be remodeled by cells. To overcome this limitation, cell-adhesion peptides[24–26] and protease-degradable peptide linkers[18,27–29] are often incorporated into the network. While the incorporation of these peptides increases the bioactivity of the material, it still does not completely recapitulate the rich bioactivity and topography of full-length proteins. Moreover, the majority of studies only incorporate the cell-adhesion peptide sequence RGDS, which interacts with a limited set of integrins, and, therefore, does not completely mimic all cell-matrix interactions present *in vivo*[30]. Conversely, naturally-derived biomaterials, specifically ECM-derived materials (e.g., collagen, reconstituted basement membrane, and fibrin), possess inherent bioactivity, but exhibit weak mechanical properties. Therefore, several efforts have been undertaken to improve the mechanical properties of ECM-derived materials; for example, with 3D collagen, the elastic moduli is increased by crosslinking with glutaraldehyde, ribose, or tissue transglutaminase[31]. However, each of these approaches has their limitations as glutaraldehyde is cytotoxic[32,33], ribose yields a limited elastic moduli range between 100 and 150 Pa[2], and tissue transglutaminase alters pore size[34,35].

A promising alternative to purely synthetic or naturally-derived biomaterials is an interpenetrating network (IPN) composed of a primary ECM-derived network reinforced by a secondary polymeric network, which yields a material possessing both inherent bioactivity and tunable mechanical properties. Here, we describe an IPN platform containing a fibrillar collagen type-I network reinforced by a secondary polymeric network formed from thiol-ene polyethylene glycol) (PEG). Specifically, we report that the PEG/Collagen IPN possesses inherent bioactivity, high cytocompatibility, and tunable mechanical properties over several orders of magnitude, thus making it a useful tool for studying mechanobiology. Furthermore, we use the PEG/Collagen IPN system to investigate the effect of mechanical confinement on cancer cell behavior, which is hypothesized to be present during early-stage tumors that have not yet invaded into the surrounding ECM[36–40]. We find that mechanical confinement inhibits malignant-like behavior in the triple negative breast cancer cell line MDA.MB.231 —as exhibited by decreases in viability, proliferation, and motility.

2. Materials and Methods

2.1 Materials and cell culture:

All chemicals were purchased from Sigma-Aldrich (St. Louis, MO) unless otherwise noted. The triple negative breast cancer cell line MDA.MB.231 (ATCC, Manassas, VA) was maintained at 37°C and 5% CO2 in DMEM (Invitrogen, Carlsbad, CA) supplemented with 10% fetal bovine serum (ThermoScientific, Logan, UT) and 1% penicillin-streptomycin until passage 15

2.2 IPN formation:

To generate the PEG/Collagen IPNs, 3D collagen gels were first generated as previously described[41,42]. Briefly, High Concentration Rat Tail Type I Collagen (Corning Life Sciences, Corning, NY) was combined in a 1:1 volumetric ratio with collagen neutralizing buffer (100 mM HEPES in 2x PBS, pH 7.3) and diluted to the appropriate working concentration in 1x PBS; in this study the collagen gel concentration was kept constant at 2 mg/mL. The collagen solution was then gelled by placing the solution in an incubator at 37°C for 1 hour. Once the collagen had fully polymerized, a solution containing the PEG monomers (10 kD PEGnorbornene (PEG4NB) (Sigma-Aldrich, St. Louis, MO) and 1 kD PEGdithiol (Creative PEGWorks, Chapel Hill, NC)), in a constant 1:2 molar ratio of PEG4NB:PEGdithiol, and 0.1 mM of the photo-initiator Eosin Y was added and allowed to diffuse into the collagen gels. Upon reaching diffusive equilibrium, excess PEG solution was removed and the surfaces of the collagen gels were washed one time with 1x PBS. The PEG network was then formed by irradiating the gels with visible laser light (514 nm, 500 mW cm^{-2}) for 120 s.

2.3 Mechanical characterization:

The mechanical properties of the PEG/Collagen IPNs were characterized using the displacement-controlled Piuma nanoindentation system (Optics11, Netherlands). Here, a spherical probe with a radius of 20.5 μm and a cantilever stiffness of 0.105 N m^{-1} was indented into the surface of the PEG/Collagen IPNs at a constant rate of 10 μm s^{-1}. The reduced elastic moduli of the IPNs were then calculated using Hertz contact theory and assuming the material to be linear elastic and isotropic. Importantly, the reduced elastic modulus was calculated on the loading portion of the load-displacement curve, which has been shown to be more suitable for soft, hydrated materials[43,44]. All measurements were performed on samples covalently anchored to a glass-bottom dish and submerged within 1x PBS. Each sample was indented five times and the probe was moved to a new location at least 500 μm away from the previous indentation location in order to avoid loading effects.

2.4 Characterization of molecular diffusion:

The diffusion properties of the well-characterized biomolecule bovine serum albumin labeled with AlexaFluor 594 (BSA-AlexaFluor 594; Invitrogen, Carlsbad, CA), which has a molecular weight of 66.6 kD, were measured within PEG/Collagen IPNs. Here, IPNs were formed within 24-well transwell inserts (Corning Life Sciences, Corning, NY) containing a polyester membrane with 0.4 μm pores and a pore density of 4×10^6 pores per cm^2. After formation of the IPNs, a solution containing the molecule of interest was added to the top of the transwell insert and allowed to diffuse into the IPN. To ensure that the molecules of interest had fully diffused into our IPNs, diffusion experiments were performed 7 days after initial addition of BSA-AlexaFluor 594.

Upon starting the diffusion experiments, 1000 μL of PBS was added to the bottom of the transwell plates and samples were taken periodically over the course of 6 hours. The diffusion kinetics were then measured using a SpectraMax M5 Plate Reader (Molecular Devices, Sunnyvale, Ca) by fluorescence at 590/617 excitation/emission. To calculate

diffusion coefficients, the semi-infinite slab approximation was used as previously described[4,12]. The method is further described in the supplementary information.

2.5 Computational modeling of PEG monomer diffusion using finite element analysis:

To better understand the diffusion kinetics of PEG monomers into the collagen gels prior to irradiation, we generated a diffusion model with COMSOL Multiphysics (COMSOL Inc., Palo Alto, USA) software. Briefly, the geometry of the collagen gels was recreated using axi-symmetric symmetry. After estimating the hydrodynamic radius of the PEG monomers, as detailed in the supplementary information, the diffusion coefficient of each PEG monomer was calculated and inputted into the COMSOL model. The PEG concentration as a function of time and z-position within collagen was then simulated.

2.6 Imaging of IPNs with scanning electron microscopy (SEM):

The IPNs were prepared for SEM using a modified approach based on a previously described technique[45,46]. Here, IPN samples were serially transitioned into absolute methanol by first treating with 30 minute incubations with 35, 50, 70, 90, and 100% ethanol. Then, two 30 min incubations of 100% methanol were performed. Methanol dehydrated IPNs were dried in a critical point dryer and adhered onto sample stubs using carbon tape. Samples were then sputter coated with 5 nm of platinum-palladium and imaged using a Carl Zeiss Supra 55 VP Field Emission Scanning Electron Microscope.

2.7 Viability analysis:

To measure the cytotoxicity of the IPN system, cell viability was measured using a LIVE/DEAD assay (ThermoFisher, Waltham, MA). For the viability experiments, single cells were first encapsulated within 2 mg/mL collagen gels and allowed to adhere overnight. Then, PEG solutions containing 0.1 mM Eosin Y were added to the top of the collagen gels and allowed to diffuse for 6 hours, at which point diffusive equilibrium was reached within our system. After 6 hours, excess PEG solution was removed and the gels were irradiated with visible light as previously described. The PEG/Collagen IPNs were then washed three times with media (1 hr for each wash) to remove unreacted monomer. For the 0 mM PEG4NB irradiated and non-irradiated conditions, Eosin Y was omitted in order to determine the effect of laser light alone on cell viability. Eosin Y is safe photoinitiating system that has been used by a number of research groups[47–50] as well as in FDA approved devices[51].

For the LIVE/DEAD assay, 2 μM of Calcein AM and 4 μM of Ethidium homodimer-1 in serum-free DMEM was added and incubated for 30 min at 37°C. Three-dimensional images (10 μm intervals for 500 μm) were then acquired using a confocal microscope. The images were analyzed in ImageJ, and the percentage of viable cells was calculated manually in a blinded manner.

2.8 Proliferation analysis:

The commercially-available Click-iT EdU (ThermoFisher, Waltham, MA) assay was used to assess the proliferation of single MDA.MB.231 cells embedded within the PEG/Collagen IPN system. After forming cell-laden PEG/Collagen IPNs, as previously described, the cells were cultured for 48 hours in normal cell culture media, at which point the cell culture

media was replaced with fresh media containing 10 μM of EdU. The cell-laden PEG/Collagen IPNs were then incubated with the EdU media for 16 hours and subsequently fixed with 4% PFA. The fixed PEG/Collagen IPNs were then prepared for EdU staining using the manufacturer's protocol. After staining with the AlexaFluor 647 azide small molecule, the samples were counterstained with Hoechst 33342 for nuclear detection.

The samples were then imaged using confocal microscopy and 150 μm stacks with 3 pm image intervals were acquired. The images were evaluated with Imaris image analysis software (Bitplane, St. Paul, MN) using its spot-detection algorithm. Briefly, a minimum intensity threshold was set for the EdU channel based on unstained controls. Then, the percentage of proliferating cells was calculated by dividing the number of EdU+ cells by the total number of nuclei identified using the spot-detection algorithm for the Hoechst 33342 channel.

2.9 Single-cell migration assay:

PEG/Collagen IPNs with MDA.MB.231 cells diffusely embedded were prepared as previously described. To record single-cell migration behavior, brightfield time-lapse images were acquired using a confocal microscope with an environmental chamber. Image acquisition began immediately following PEG/Collagen IPN crosslinking and images were acquired every 10 min for 24 hours.

The time-lapse images were analyzed using a custom-written ImageJ routine in combination with Imaris image analysis software. Three-dimensional bright-field images were projected in the z-direction using the minimum pixel intensity value and inverted. The resulting z-projected image was then imported into Imaris, and the spot-tracking algorithm was used to track the z-projected motion of individual cells.

2.10 Spheroid invasion assay:

Spheroids were formed as previously described[41,42] with one exception; 96-well ultra-low attachment plates (Corning) were used instead of agarose-coated plates. The spheroids were then embedded within 2 mg/mL collagen gels and allowed to adhere for 24 hours. PEG solutions were then added and allowed to diffuse for 6 hours, after which excess PEG solution was removed and the gels were irradiated with visible light. The gels were then washed three times with media to remove any unreacted monomers. Spheroid size was then recorded by taking brightfield images at Day −1, 0, 1, 3, 5, and 7. To quantify the radius of the invasive edge of spheroids, we adapted a previously developed computational method[52], which utilizes the magnitude of the gradient of brightfield images, and is further described in the supplementary information.

2.11 Microscopy:

Images were acquired on a DMI600B microscope (Leica, Wetzlar, Germany) with an ImagEM EM-CCD Camera (Hamamatsu Photonics, Hamamatsu, Japan) in a spinning disc confocal setup (Yokogawa) with a LIVECELL environmental chamber (Pathology Devices, San Diego, CA). Imaging was performed with Micro-Manager 1.4 Software (http://www.micro-manager.org).

2.12 Statistical analysis

All statistical data were expressed as mean ± standard deviation. Statistical analysis was carried out by one-way ANOVA with Tukey-Kramer post hoc test. A value of $p < 0.05$ was considered statistically significant.

3. Results and Discussion

3.1 PEG/Collagen IPN design rationale:

To generate a 3D *in vitro* cell culture system possessing both inherent bioactivity and tunable mechanical properties, we developed an IPN composed of a collagen type-I primary network reinforced with a secondary PEG thiol-ene network (Fig. 1a). We anticipated that the naturally-derived collagen type-I network would provide inherent bioactivity via its fibrillar architecture and cellular-adhesion cues while the synthetic PEG thiol-ene secondary network would provide robust, tunable mechanical properties. However, because parameters such as pH, temperature, and the ionic strength of the buffer solution can affect the collagen fiber architecture during collagen gel formation[53,54], we first formed the collagen network, then delivered the soluble PEG monomers to the collagen network, and subsequently crosslinked the PEG monomers into a secondary network via visible light *in situ* (Fig. 1b and 1c). Such an approach ensured that the IPN system contained a fibrillar collagen network, thus mimicking the *in vivo* ECM architecture, while also possessing a secondary PEG network.

The design criteria for our IPN included the ability to: 1) form networks from monomers capable of readily diffusing into cell-laden 3D collagen gels; 2) provide spatiotemporal control of crosslinking; 3) generate a stable secondary network upon crosslinking; and 4) minimally affect cell viability. To achieve these design specifications, we utilized thiol-ene “click” chemistry and explored PEG networks containing 4-arm poly(ethylene glycol) monomers functionalized with norbornene (PEG4NB) and linear poly(ethylene glycol) dithiol (PEGdithiol) as a crosslinker (Fig 1c). Importantly, because the PEG monomers were of low molecular weight (less than 10 kD), the monomers readily diffused into collagen gels, thus satisfying our first design criterion (See supplementary information and Fig. S1 for further details).

PEG thiol-ene “click” chemistry has previously been used in 3D cell culture systems owing to its ability to proceed rapidly under mild conditions, react in the presence of oxygen, generate homogeneous networks, and be cytocompatible[55–57]. Additionally, these reactions are considered bio-orthogonal as the reagents do not react with common biological functional groups on proteins[58]. In this study, we utilized the ring-strained, and thus highly reactive, functional group norbornene (Fig. 1c)[59].

To achieve spatiotemporal control of the reaction, the PEG thiol-ene crosslinking reaction was initiated using the visible light photoinitiator Eosin Y in combination with green laser light from a medical-grade laser. Using a visible light photoinitiator circumvents concerns associatedwith UV initiators; namely potential DNA damage and reduced long-term cell viability[60]. Moreover, Eosin Y is a type II photoinitiator that often requires a potentially cytotoxic coinitiator (e.g. triethanolamine) and comonomer (e.g. 1-vinyl-2 Pyrrolidinone) to

initiate crosslinking (Fig. S2)[61]. However, due to the unique step-growth mechanism of thiol-ene chemistry, co-initiators and co-monomers are excluded as Eosin Y can abstract a hydrogen atom from the sulfihydryl group on the PEGdithiol monomer generating a thiyl radical and initiating crosslinking[62]. Consequently, the use of Eosin Y as the photoinitiator provides a high degree of spatiotemporal without adversely affecting cellular viability (Fig. S2).

3.2 PEG/Collagen IPN mechanical testing:

The generation of a stable secondary thiol-ene PEG network was confirmed via nanoindentation mechanical testing as the PEG/Collagen IPN system exhibited a tunable elastic modulus over several orders of magnitude: ranging from ~40 Pa for PEG/Collagen IPNs with 5 mM PEG4NB to ~4 kPa for PEG/Collagen IPNs with 10 mM PEG4NB, as shown in Fig. 2a. Notably, this range encompasses the elastic moduli of normal mammary gland tissue (~200 Pa) and cancerous breast tissue (~1,600 Pa)[2], and is a significant improvement in mechanical properties compared to the collagen-only controls, which possess an elastic moduli of ~10 Pa and this value is in accordance with prior literature[63,64]. In addition, the crosslinking time was inversely related to PEG monomer concentration as the 5 mM and 10 mM PEG4NB conditions fully crosslinked after 45 s and 7.5 s, respectively (Figure S3). Moreover, the elastic modulus could be further increased to ~18 kPa by lowering the molecular weight of the PEGdithiol crosslinker to 0.154 kD (Fig. S4). However, the 1 kD PEGdithiol was used for all studies as the shorter crosslinker adversely affected cell viability (Fig. S5 and S6).

3.3 PEG/Collagen IPN biomolecular transport analysis

Prior to performing the cell studies, we investigated if the additional PEG secondary network within the PEG/Collagen IPN alters the microstructure compared to a collagen-only network as the pore size of PEG and collagen networks have different length scales: pure collagen networks have pore sizes on the order of a few micrometers[65], while pure PEG hydrogels typically have pore sizes on the order of nanometers[66,67]. Thus, we expected that the altered microstructure in the PEG/Collagen IPN condition may slow the diffusion of biomolecules. The diffusion kinetics of fluorescently-labeled bovine serum albumin (BSA) molecules were measured as BSA diffused from BSA-laden networks, and the diffusion coefficient within each of our networks was determined by fitting the data to a semi-infinite slab approximation diffusion model (Fig. S7). The results revealed that the PEG/Collagen IPNs significantly impair diffusion compared to the collagen-only control (Fig. 2b). The BSA diffusion coefficient within 2 mg/mL collagen was $1.01 \pm 0.19 \times 10^{-7}$ cm^2/s, and decreased to $7.25 \pm 2.84 \times 10^{-9}$ cm^2/s, $3.87 \pm 2.5 \times 10^{-9}$ cm^2/s, and $2.74 \pm 1.3 \times 10^{-9}$ cm^2/s for the 5 mM, 7.5 mM, and 10 mM PEG4NB IPNs, respectively. The lower diffusion coefficients observed in the IPN treated collagen gels reflect the decrease in the porosity of the overall network due to the PEG. Notably, the diffusion coefficient was not statistically different between IPN conditions, suggesting that the IPN microstructure (i.e. pore size) does not significantly change across IPN PEG concentrations, despite orders of difference in mechanical properties. This indicates that the largest difference between PEG/Collagen IPNs with low (5 mM) and high (10 mM) PEG concentrations is primarily mechanical.

3.4 SEM imaging of PEG/Collagen IPN microstructure

To further investigate IPN/collagen microstructure, we performed scanning electron microscopy (SEM) imaging. SEM imaging showed the collagen-only sample to be highly porous and fibrillar, as expected (Fig. 2c), but the presence of the secondary PEG network in the 10 mM PEG4NB/collagen sample afforded a less porous microstructure (Fig. 2d). For the pure 10 mM PEG4NB network, the gel appeared as a continuous surface due to its pore size being on the order of nanometers (Fig. 2e). Analyzing the SEM images by generating histograms of pixel-intensity reflected these observed differences in microstructure as well. The histogram for the collagen condition (Fig. 2f) displayed a left-shifted curve, indicating that the microstructure is highly porous and heterogeneous. Interestingly, the histogram for the PEG/Collagen IPN condition (Fig. 2g) appeared to be more normalized, reflecting that the secondary PEG network yields a less porous and more homogeneous microstructure. The histogram for the pure PEG condition (Fig. 2h) showed a narrow peak, illustrating a very homogeneous network microstructure.

3.5 PEG/Collagen IPN cellular experiments rationale:

In two-dimensional studies, softer substrates inhibit cell spreading and promote apoptosis as compared to stiffer substrates[68]. However, in our PEG/Collagen IPN platform, we predicted that increasing the stiffness of the network in the absence of cell-degradable crosslinkers may mechanically confine cells and impair viability as well as proliferation. Therefore, we assessed the cellular response of the metastatic breast cancer cell line MDA.MB.231 when embedded as single cells within PEG/Collagen IPNs according to the protocol illustrated in Fig. 3a. In addition, finite element modeling of the PEG monomer diffusion kinetics in our 3D collagen gels revealed that diffusive equilibrium is reached within 6 hours (Fig. 3b). As a result, the PEG monomers were allowed to diffuse into the cell-laden collagen gels for 6 hours, after which the gels were exposed to green laser light and crosslinked.

3.6 PEG/Collagen IPN viability assay

Cellular viability was assessed 24 hours after IPN crosslinking and an inverse relationship between MDA.MB.231 cell viability and PEG4NB concentration was observed within the PEG/Collagen IPN. Cell viabilities were found to be 88.4 ± 0.4, 84.8 ± 1.7, 76.8 ± 4.0, and 74.9 ± 1.1% (mean ± S.D.; n = 3) for PEG/Collagen IPNs with 0, 5, 7.5, and 10 mM PEG4NB, respectively (Fig. 3c-g). To determine whether this decrease in viability was due to mechanical confinement or a chemical effect from the soluble monomers, we performed the control in which the monomer solutions were added to the cell-laden collagen gels, but not irradiated. In the non-irradiated controls, the viabilities were 95.0 ± 3.2, 95.6 ± 2.3, 97.2 ± 1.96, and 97.2 ± 0.6% (mean ± S.D.; n = 3) for polymer solutions containing 0, 5, 7.5, and 10 mM PEG4NB, respectively (Fig. 3g). In addition, the viability of the irradiated 0 mM PEG4NB, which did not contain Eosin Y, was not significantly different from the non-irradiated 0 mM PEG4NB control; indicating that the laser light alone does not affect cellular viability (Fig. 3g).

The results also suggest that the observed differences in viability are not attributable to free radicals. If free radicals were affecting cellular viability, cellular viability would increase

with increasing PEG4NB concentration due to higher PEG4NB concentrations having shorter crosslinking times (Fig. S3). However, we observe the opposite trend, which suggests that the decrease in viability exhibited by the crosslinked PEG/Collagen IPN conditions is not a consequence of free radicals. Furthermore, the observed decreases in viability within the crosslinked conditions are also unlikely to be attributable to the monomers interacting with proteins on the surface of cells as this has not been previously reported[18,19,57]. Moreover, if the monomers were reacting with cells, we would likely observe a failure in the formation of the secondary network because the stoichiometric ratio between norbornene and thiols would be altered, and step-growth reactions such as the thiol-ene reaction are sensitive to stoichiometric changes as predicted by the Flory-Stockmayer equation[69,70]. However, we observe good network formation, therefore suggesting that the reduced viability is not due to the monomers directly interacting with cells, but is instead a mechanical effect.

3.7 PEG/Collagen IPN proliferation assay

To assess proliferation within the IPN system, the EdU assay was employ ed 72 hours after IPN formation. The proliferation assay revealed that mechanically confining cells within the PEG/Collagen IPN platform significantly decreased the proliferation rate as the percentage of EdU^+ cells decreased from 72.8 ± 8.3, to 12.9 ± 15.0, 12.97 ± 15.4, and to 3.0 ± 6.1% (mean ± S.D.; n = 3 gels, 4 locations per gel) for the 0, 5, 7.5, and 10 mM PEG4NB IPN networks, respectively (Fig. 3h). Again, to confirm that these results were due to mechanical effects and not chemical, we performed the control in which the PEG monomer solutions were added, but not irradiated. The percentage of EdU^+ cells were determined to be 73.4 ± 10.9, 73.9 ± 20.9, 76.2 ± 12.4, and 61.0 ± 18.9% (mean ± S.D.; n = 3 gels, 4 locations per gel) for 0, 5, 7.5, and 10 mM PEG4NB, respectively (Fig. 3h). Notably, proliferation in the irradiated 0 mM PEG4NB condition, which did not contain Eosin Y, was not significantly different from the non-irradiated 0 mM PEG4NB control; showing that laser light alone does not affect cellular proliferation. Therefore, the decrease in proliferation is due to mechanical confinement from the crosslinked PEG network and not a result from the soluble monomers prior to crosslinking.

In addition, we found that mechanically confining cells within a secondary PEG network was more effective at inhibiting proliferation than serum-starvation (Fig. 3i). Cells embedded within 2 mg/mL collagen gels were serum-starved beginning at the same time point as when the other conditions began receiving the soluble monomer solutions. While serum-depletion did elicit a decrease in proliferation, 58.8 ± 11.0% (mean ± S.D.; n = 3 gels, 4 locations per gel), the percentage of EdU^+ cells remained significantly higher compared to the PEG/Collagen IPN conditions, indicating that mechanical confinement of MDA.MB.231 cells is more effective at inhibiting proliferation than removal of growth factors.

3.8 PEG/Collagen IPN single-cell migration assay

In order to confirm that the cells were being confined by the presence of the secondary PEG network within our PEG/Collagen IPN system, we assessed the migratory behavior of single MDA.MB.231 cells embedded within the IPN system. The single-cell migration assays showed that cells embedded within the PEG/Collagen IPN platform were essentially

immobilized (Fig. 4a and Movie 1–2) as cell speeds were less than 15 pm/hr. This value represents cells that are essentially oscillating in place and not translocating. Importantly, cells in the non-irradiated control displayed no significant difference in cell speed across all polymer concentrations. For the irradiated PEG/Collagen IPN conditions, mean cell speed of the entire population was 22.5 ± 0.9, 11.6 ± 0.9, 7.5 ± 0.5, and 7.7 ± 0.3 μm/hr for the 0, 5, 7.5, and 10 mM PEG4NB, respectively (Fig. 4b). However, the mean cell speeds for the non-irradiated controls were not statistically different from each other, and were 23.9 ± 0.4, 23.7 ± 0.30, 23.7 ± 0.30, and 23.8 ± 0.26 μm/hr for 0, 5, 7.5, and 10 mM PEG4NB, respectively (Fig. 4b). These results indicate that the PEG/Collagen IPNs, without cell-degradable crosslinkers, physically constrain cells and inhibit their migration. Moreover, the results from the non-irradiated controls suggest that this lack of motion is due to mechanical confinement and not a chemical effect resulting from the soluble monomers prior to crosslinking.

The inhibitory effect of PEG/Collagen IPNs on single-cell migration led us to investigate whether this inhibitory behavior is also be present within an embedded multicellular spheroid model, which better mimics the *in vivo* multicellular architecture compared to single cells diffusely embedded within collagen as it recapitulates critical cell-cell interactions[41,71]. The results revealed that adding a secondary, non-degradable PEG network impaired MDA.MB.231 spheroid invasion into the surrounding matrix (Fig. 4c and Movie 3). Furthermore, the non-irradiated controls displayed significant invasion, indicating that this result was due to a mechanical effect and not a chemical effect from the soluble monomers prior to crosslinking (Fig. 4c and Movie 4). Eventually, narrow protrusions from the spheroid did develop within the PEG/Collagen IPN conditions, likely due to hydrolytic cleavage of the PEG4NB molecule at later time points, but the overall number of invading cells appeared to be significantly less than the control. Therefore, these results show that the PEG/Collagen IPN platform mechanically confines spheroids and inhibits their invasion.

4. Conclusions

The PEG/Collagen IPN combines the inherent bioactivity of native collagen networks (i.e., native cell-adhesion sites and topology of full-length collagen proteins) with the tunable mechanical properties of synthetic PEG networks. Moreover, because the soluble monomers are first delivered to the cell-laden collagen network and then crosslinked into a 3D network via visible light, this approach maintains the collagen network's fibrillar architecture and allows for the effects of network mechanics to be studied independently of collagen density. Furthermore, we show that the PEG/Collagen IPN platform is cytocompatible, inherently bioactive, and mechanically tunable over several orders of magnitude, spanning the stiffness range between normal and malignant breast tissue[1].

We also demonstrate that mechanically confining cancer cells via our PEG/Collagen IPN platform impairs behavior characteristic of malignant cells, which is in agreement with prior work using agarose[72,73]. However, agarose lacks cell-adhesion sites. Therefore, our PEG/Collagen IPN platform is an improvement upon earlier models as it enables mechanical confinement of cancer cells while also providing cell-adhesion cues, which is more reflective of the *in vivo* tumor microenvironment. Furthermore, our results also reflect

previous two-dimensional studies showing that confinement via micropatterned substrates promotes apoptosis and inhibits proliferation via decreased cytoskeletal tension[74–77].

With respect to *in vivo* tumors, it is currently unclear how mechanical confinement, and the solid stress that develops, affects cancer progression. While we observe that mechanical confinement inhibits malignant-like behavior, others have hypothesized that solid stress may promote malignancy via the collapse of blood vessels and formation of a hypoxic environment[36,37,40,78]. Consequently, significant gaps in knowledge remain with respect to mechanically-confined tumors *in vivo*, and our PEG/Collagen IPN is a tool that fulfills a number of the current gaps.

Supplementary Material

Refer to Web version on PubMed Central for supplementary material.

Acknowledgements

The authors would like to thank Dr. Jason Christopher and Ms. Anlee Krupp for assistance with SEM imaging. This work was supported in part by 1U01 CA202123 (M.H.Z), P01HL 120839 (M.H.Z), T32 EB006359 (M.W.G, D.S.R)[79], a National Science Foundation Graduate Research Fellowship GRF DGE-1247312 (D.S.R), and the Kenneth R. Lutchen Distinguished Summer Fellowship (K.M.B). The authors declare that they have no competing interests.

References

[1]. Paszek MJ, Zahir N, Johnson KR, Lakins JN, Rozenberg GI, Gefen A, Reinhart-King CA, Margulies SS, Dembo M, Boettiger D, Hammer DA, Weaver VM, Tensional homeostasis and the malignant phenotype., Cancer Cell. 8 (2005) 241–54. doi:10.1016/j.ccr.2005.08.010. [PubMed: 16169468]

[2]. Levental KR, Yu H, Kass L, Lakins JN, Egeblad M, Erler JT, Fong SFT, Csiszar K, Giaccia A, Weninger W, Yamauchi M, Gasser DL, Weaver VM, Matrix crosslinking forces tumor progression by enhancing integrin signaling., Cell. 139 (2009) 891–906. doi:10.1016/j.cell.2009.10.027. [PubMed: 19931152]

[3]. Spill F, Reynolds DS, Kamm RD, Zaman MH, Impact of the physical microenvironment on tumor progression and metastasis, Curr. Opin. Biotechnol 40 (2016) 41–48. doi:10.1016/j.copbio.2016.02.007. [PubMed: 26938687]

[4]. Chaudhuri O, Koshy ST, Branco da Cunha C, Shin J-W, Verbeke CS, Allison KH, Mooney DJ, Extracellular matrix stiffness and composition jointly regulate the induction of malignant phenotypes in mammary epithelium, Nat. Mater 13 (2014) 1–35. doi: 10.1038/nmat4009. [PubMed: 24343503]

[5]. Sapudom J, Rubner S, Martin S, Kurth T, Riedel S, Mierke CT, Pompe T, The phenotype of cancer cell invasion controlled by fibril diameter and pore size of 3D collagen networks, Biomaterials. 52 (2015) 367–375. doi: 10.1016/j.biomaterials.2015.02.022. [PubMed: 25818443]

[6]. Nam S, Hu KH, Butte MJ, Chaudhuri O, Strain-enhanced stress relaxation impacts nonlinear elasticity in collagen gels, Proc. Natl. Acad. Sci 113 (2016) 5492–5497. doi: 10.1073/pnas.1523906113. [PubMed: 27140623]

[7]. Eyckmans J, Boudou T, Yu X, Chen CS, A Hitchhiker's Guide to Mechanobiology, Dev. Cell 21 (2011)35–47. doi: 10.1016/j.devcel.2011.06.015. [PubMed: 21763607]

[8]. Engler AJ, Sen S, Sweeney HL, Discher DE, Matrix Elasticity Directs Stem Cell Lineage Specification, Cell. 126 (2006) 677–689. doi: 10.1016/j.cell.2006.06.044. [PubMed: 16923388]

[9]. Lo CM, Wang HB, Dembo M, Wang YL, Cell movement is guided by the rigidity of the substrate., Biophys. J 79 (2000) 144–52. doi:10.1016/S0006-3495(00)76279-5. [PubMed: 10866943]

[10]. Yeung T, Georges PC, Flanagan LA, Marg B, Ortiz M, Funaki M, Zahir N, Ming W, Weaver V, Janmey PA, Effects of substrate stiffness on cell morphology, cytoskeletal structure, and adhesion, Cell Motif Cytoskeleton. 60 (2005) 24–34. doi: 10.1002/cm.20041.

[11]. Discher DE, Janmey P, Wang Y-L, Tissue cells feel and respond to the stiffness of their substrate., Science. 310 (2005) 1139–43. doi:10.1126/science.1116995. [PubMed: 16293750]

[12]. Huebsch N, Arany PR, Mao AS, Shvartsman D, Ali OA, Bencherif SA, Rivera-Feliciano J, Mooney DJ, Harnessing traction-mediated manipulation of the cell/matrix interface to control stem-cell fate., Nat. Mater 9 (2010) 518–26. doi:10.1038/nmat2732. [PubMed: 20418863]

[13]. Wirtz D, Konstantopoulos K, Searson PCPCPC, The physics of cancer: the role of physical interactions and mechanical forces in metastasis, Nat. Rev. Cancer 11 (2011) 522. doi: 10.1038/nrc3080.

[14]. Fraley SI, Wu P, He L, Feng Y, Krisnamurthy R, Longmore GD, Wirtz D, Three-dimensional matrix fiber alignment modulates cell migration and MT1-MMP utility by spatially and temporally directing protrusions, Sci. Rep 5 (2015) 14580. [PubMed: 26423227]

[15]. Zaman MH, Trapani LM, Sieminski AL, MacKellar D, Gong H, Kamm RD, Wells A, Lauffenburger DA, Matsudaira P, Migration of tumor cells in 3D matrices is governed by matrix stiffness along with cell-matrix adhesion and proteolysis, Proc. Natl. Acad. Sci. 103 (2006) 10889–10894. doi:10.1073/pnas.0604460103. [PubMed: 16832052]

[16]. Wozniak MA, Desai R, Solski PA, Der CJ, Keely PJ, ROCK-generated contractility regulates breast epithelial cell differentiation in response to the physical properties of a three-dimensional collagen matrix, J. Cell Biol 163 (2003) 583–595. doi: 10.1083/jcb.200305010. [PubMed: 14610060]

[17]. Doyle AD, Wang FW, Matsumoto K, Yamada KM, One-dimensional topography underlies three-imensional fibrillar cell migration, J. Cell Biol 184 (2009) 481–490. doi: 10.1083/jcb.200810041. [PubMed: 19221195]

[18]. Schwartz MP, Fairbanks BD, Rogers RE, Rangarajan R, Zaman MH, Anseth KS, A synthetic strategy for mimicking the extracellular matrix provides new insight about tumor cell migration., Integr. Biol. (Camb) 2 (2010) 32–40. doi:10.1039/b912438a. [PubMed: 20473410]

[19]. Schwartz MP, Rogers RE, Singh SP, Lee JY, Loveland SG, Koepsel JT, Witze ES, Montanez-Sauri SI, Sung KE, Tokuda EY, Sharma Y, Everhart LM, Nguyen EH, Zaman MH, Beebe DJ, Ahn NG, Murphy WL, Anseth KS, A Quantitative Comparison of Human HT-1080 Fibrosarcoma Cells and Primary Human Dermal Fibroblasts Identifies a 3D Migration Mechanism with Properties Unique to the Transformed Phenotype., PLoS One. 8 (2013) e81689. doi:10.1371/journal.pone.0081689. [PubMed: 24349113]

[20]. Ulrich TA, Jain A, Tanner K, MacKay JL, Kumar S, Probing cellular mechanobiology in three-dimensional culture with collagen-agarose matrices, Biomaterials. 31 (2010) 1875–1884. doi: 10.1016/j.biomaterials.2009.10.047. [PubMed: 19926126]

[21]. Berger AJ, Linsmeier KM, Kreeger PK, Masters KS, Decoupling the effects of stiffness and fiber density on cellular behaviors via an interpenetrating network of gelatin-methacrylate and collagen, Biomaterials. 141 (2017) 125–135. doi: 10.1016/j.biomaterials.2017.06.039. [PubMed: 28683337]

[22]. Tibbitt MW, Anseth KS, Hydrogels as extracellular matrix mimics for 3D cell culture, Biotechnol. Bioeng 103 (2009) 655–663. doi: 10.1002/bit.22361. [PubMed: 19472329]

[23]. Burdick JA, Anseth KS, Photoencapsulation of osteoblasts in injectable RGD-modified PEG hydrogels for bone tissue engineering, Biomaterials. 23 (2002) 4315–4323. doi: 10.1016/SO142-9612(02)00176-X. [PubMed: 12219821]

[24]. Lee ST, L Yun J, Jo YS, Mochizuki M, van der Vlies AJ, Kontos S, Ihm JE, Lim JM, Hubbell JA, Engineering integrin signaling for promoting embryonic stem cell self-renewal in a precisely defined niche, Biomaterials. 31 (2010) 1219–1226. doi: 10.1016/j.biomaterials.2009.10.054. [PubMed: 19926127]

[25]. Benoit DSW, Anseth KS, The effect on osteoblast function of colocalized RGD and PHSRN epitopes on PEG surfaces, Biomaterials. 26 (2005) 5209–5220. doi: 10.1016/j.biomaterials.2005.01.045. [PubMed: 15792548]

[26]. Benoit DSW, Schwartz MP, Durney AR, Anseth KS, Small functional groups for controlled differentiation of hydrogel-encapsulated human mesenchymal stem cells., Nat. Mater 7 (2008) 816–23. doi:10.1038/nmat2269. [PubMed: 18724374]

[27]. Lutolf MP, Doyonnas R, Havenstrite K, Koleckar K, Blau HM, Perturbation of single hematopoietic stem cell fates in artificial niches., Integr. Biol. (Camb) 1 (2009) 59–69. doi: 10.1039/b815718a. [PubMed: 20023792]

[28]. Patterson J, Hubbell JA, Enhanced proteolytic degradation of molecularly engineered PEG hydrogels in response to MMP-1 and MMP-2, Biomaterials. 31 (2010) 7836–7845. doi: 10.1016/j.biomaterials.2010.06.061. [PubMed: 20667588]

[29]. Ehrbar M, Sala A, Lienemann P, Ranga A, Mosiewicz K, Bittermann A, Rizzi SC, Weber FE, Lutolf MP, Elucidating the role of matrix stiffness in 3D cell migration and remodeling, Biophys. J 100 (2011) 284–293. doi: 10.1016/j.bpj.2010.11.082. [PubMed: 21244824]

[30]. Ruoslahti E, RGD and Other Recognition Sequences for Integrins, Annu. Rev. Cell Dev. Biol 12(1996) 697–715. doi:10.1146/annurev.cellbio.12.1.697. [PubMed: 8970741]

[31]. Parenteau-Bareil R, Gauvin R, Berthod F, Collagen-Based Biomaterials for Tissue Engineering Applications, Materials (Basel). 3 (2010) 1863–1887. doi: 10.3390/ma3031863.

[32]. Olde Damink LHH, Dijkstra PJ, Van Luyn MJA, Van Wachem PB, Nieuwenhuis P, Feijen J, Glutaraldehyde as a crosslinking agent for collagen-based biomaterials, J. Mater. Sci. Mater. Med 6 (1995) 460–472. doi:10.1007/BF00123371.

[33]. Gough JE, Scotchford CA, Downes S, Cytotoxicity of glutaraldehyde crosslinked collagen/poly(vinyl alcohol) films is by the mechanism of apoptosis, J. Biomed. Mater. Res 61 (2002) 121–130. doi: 10.1002/jbm.10145. [PubMed: 12001254]

[34]. Mammoto A, Connor KM, Mammoto T, Yung CW, Huh D, Aderman CM, Mostoslavsky G, Smith LEH, Ingber DE, A mechanosensitive transcriptional mechanism that controls angiogenesis, Nature. 457 (2009) 1103–1108. doi:10.1038/nature07765. [PubMed: 19242469]

[35]. Boyd-White J, Williams JC, Effect of cross-linking on matrix permeability: A model for AGE-modified basement membranes, Diabetes. 45 (1996) 348–353. doi: 10.2337/diab.45.3.348. [PubMed: 8593941]

[36]. Stylianopoulos T, Martin JD, Chauhan VP, Jain SR, Diop-Frimpong B, Bardeesy N, Smith BL, Ferrone CR, Homicek FJ, Boucher Y, Munn LL, Jain RK, Causes, consequences, and remedies for growth-induced solid stress in murine and human tumors, Proc. Natl. Acad. Sci 109 (2012) 15101–15108. doi: 10.1073/pnas.1213353109. [PubMed: 22932871]

[37]. Stylianopoulos T, Martin JD, Snuderl M, Mpekris F, Jain SR, Jain RK, Coevolution of Solid Stress and Interstitial Fluid Pressure in Tumors During Progression: Implications for Vascular Collapse, Cancer Res. 73 (2013) 3833–3841. doi:10.1158/0008-5472.CAN-12-4521. [PubMed: 23633490]

[38]. Balzer EM, Tong Z, Paul CD, Hung WC, Stroka KM, Boggs AE, Martin SS, Konstantopoulos K, Physical confinement alters tumor cell adhesion and migration phenotypes, FASEB J. 26 (2012) 4045–4056. doi: 10.1096/fj.12-211441. [PubMed: 22707566]

[39]. Demou ZN, Gene expression profiles in 3D tumor analogs indicate compressive strain differentially enhances metastatic potential, Ann. Biomed. Eng 38 (2010) 3509–3520. doi: 10.1007/sl0439-010-0097-0. [PubMed: 20559731]

[40]. Nia HT, Liu H, Seano G, Datta M, Jones D, Rahbari N, Incio J, Chauhan VP, Jung K, Martin JD, Askoxylakis V, Padera TP, Fukumura D, Boucher Y, Hornicek FJ, Grodzinsky AJ, Baish JW, Munn LL, Jain RK, Solid stress and elastic energy as measures of tumour mechanopathology, Nat. Biomed. Eng 1 (2017). doi: 10.1038/s41551-016-0004.

[41]. Reynolds DS, Tevis KM, Blessing WA, Colson YL, Zaman MH, Grinstaff MW, Breast Cancer Spheroids Reveal a Differential Cancer Stem Cell Response to Chemotherapeutic Treatment, Sci. Rep 7 (2017) 10382. doi:10.1038/s41598-017-10863-4. [PubMed: 28871147]

[42]. Charoen KM, Fallica B, Colson YL, Zaman MH, Grinstaff MW, Embedded multicellular spheroids as a biomimetic 3D cancer model for evaluating drug and drug-device combinations., Biomaterials. 35 (2014) 2264–71. doi: 10.1016/j.biomaterials.2013.11.038. [PubMed: 24360576]

[43]. Oyen ML, Mechanical characterisation of hydrogel materials, Int. Mater. Rev 59 (2014) 44–59. doi: 10.1179/1743280413Y.0000000022.

[44]. Mattel G, Gruca G, Rijnveld N, Ahluwalia A, The nano-epsilon dot method for strain rate viscoelastic characterisation of soft biomaterials by spherical nano-indentation, J. Mech. Behav. Biomed. Mater 50 (2015) 150–159. doi:10.1016/j.jmbbm.2015.06.015. [PubMed: 26143307]

[45]. Chaudhuri O, Gu L, Klumpers D, Darnell M, Bencherif SA, Weaver JC, Huebsch N, Lee H-P, Lippens E, Duda GN, Mooney DJ, Hydrogels with tunable stress relaxation regulate stem cell fate and activity., Nat. Mater 15 (2015) 326–333. doi: 10.1038/nmat4489. [PubMed: 26618884]

[46]. Branco da Cunha C, Klumpers DD, Li WA, Koshy ST, Weaver JC, Chaudhuri O, Granja PL, Mooney DJ, Influence of the stiffness of three-dimensional alginate/collagen-I interpenetrating networks on fibroblast biology, Biomaterials. 35 (2014) 8927–8936. doi: 10.1016/j.biomaterials.2014.06.047. [PubMed: 25047628]

[47]. Shih H, Lin CC, Cross-linking and degradation of step-growth hydrogels formed by thiol-ene photoclick chemistry, Biomacromolecules. 13 (2012) 2003–2012. doi: 10.1021/bm300752j. [PubMed: 22708824]

[48]. a DeForest C, Anseth KS, Cytocompatible click-based hydrogels with dynamically tunable properties through orthogonal photoconjugation and photocleavage reactions., Nat. Chem 3 (2011)925–31. doi:10.1038/nchem,1174. [PubMed: 22109271]

[49]. Bahney CS, Lujan TJ, Hsu CW, Bottlang M, West JL, Johnstone B, Visible light photoinitiation of mesenchymal stem cell-laden bioresponsive hydrogels, Eur. Cells Mater 22 (2011) 43–55. doi: 10.22203/eCM.v022a04.

[50]. Cruise GM, Hegre OD, Scharp DS, Hubbell JA, A sensitivity study of the key parameters in the interfacial photopolymerization of poly(ethylene glycol) diacrylate upon porcine islets, Biotechnol. Bioeng 57 (1998) 655–665. doi:10.1002/(SICI)1097-0290(19980320)57:6<655::AID-BIT3>3.0.CO;2-K. [PubMed: 10099245]

[51]. U.S. Food and Drug Administration, Premarket Approval for Focal Seal-L Synthetic Absorbable Sealant, Genzyme, (2000). https://www.accessdata.fda.gov/scripts/cdrh/cfdocs/cfpma/pma.cfm?id=P990028.

[52]. Stein AM, Demuth T, Mobley D, Berens M, Sander LM, A Mathematical Model of Glioblastoma Tumor Spheroid Invasion in a Three-Dimensional In Vitro Experiment, Biophys. J 92 (2007) 356–365. doi:10.1529/biophysj.106.093468. [PubMed: 17040992]

[53]. Gross J, Kirk D, The heat precipitation of collagen from neutral salt solutions: some rateregulating factors., J. Biol. Chem 233 (1958) 355–360. [PubMed: 13563501]

[54]. Wood GC, Keech MK, The formation of fibrils from collagen solutions 1. The effect of experimental conditions: kinetic and electron-microscope studies, Biochem. J 75 (1960) 588–598. doi: 10.1042/bj0750588. [PubMed: 13845809]

[55]. Kolb HC, Finn MG, Sharpless KB, Click Chemistry: Diverse Chemical Function from a Few Good Reactions, Angew. Chemie - Int. Ed 40 (2001) 2004–2021. doi: 10.1002/1521-3773(20010601)40:1l<2004::AID-ANIE2004>3.0.CO;2-5.

[56]. Barner-Kowollik C, Du Prez FE, Espeel P, Hawker CJ, Junkers T, Schlaad H, Van Camp W, “Clicking” polymers or just efficient linking: What is the difference?, Angew. Chemie - Int. Ed 50 (2011) 60–62. doi:10.1002/anie.201003707.

[57]. Azagarsamy MA, Anseth KS, Bioorthogonal click chemistry: An indispensable tool to create multifaceted cell culture scaffolds, ACS Macro Lett. 2 (2013) 5–9. doi: 10.1021/mz300585q. [PubMed: 23336091]

[58]. Tibbitt MW, Anseth KS, Dynamic microenvironments: the fourth dimension., Sci. Transl. Med 4 (2012) 160ps24. doi: 10.1126/scitranslmed.3004804.

[59]. Hoyle CE, Bowman CN, Thiol-ene click chemistry, Angew. Chemie - Int. Ed 49 (2010) 1540–1573. doi:10.1002/anie.200903924.

[60]. Sinha RP, Hader D-P, UV-induced DNA damage and repair: a review, Photochem. {&} Photobiol. Sci 1 (2002)225–236. doi:10.1039/b201230h. [PubMed: 12661961]

[61]. Cooper BG, Stewart RC, Burstein D, Snyder BD, Grinstaff MW, A Tissue-Penetrating Double Network Restores the Mechanical Properties of Degenerated Articular Cartilage, Angew. Chemie - Int. Ed 55 (2016) 4226–4230. doi:10.1002/anie.201511767.

[62]. Shih H, Lin CC, Visible-light-mediated thiol-ene hydrogelation using eosin-Y as the only photoinitiator, Macromol. Rapid Commun 34 (2013) 269–273. doi: 10.1002/marc.201200605. [PubMed: 23386583]

[63]. Forgacs G, Newman SA, Hinner B, Maier CW, Sackmann E, Assembly of Collagen Matrices as a Phase Transition Revealed by Structural and Rheologic Studies, Biophys. J 84 (2003) 1272–1280. doi:10.1016/S0006-3495(03)74942-X. [PubMed: 12547807]

[64]. Willits RK, Skomia SL, Effect of collagen gel stiffness on neurite extension, J. Biomater. Sci. Polym. Ed 15 (2004) 1521–1531. doi: 10.1163/1568562042459698. [PubMed: 15696797]

[65]. Haijanto D, Maffei JS, Zaman MH, Quantitative analysis of the effect of cancer invasiveness and collagen concentration on 3D matrix remodeling, PLoS One. 6 (2011). doi: 10.1371/journal.pone.0024891.

[66]. Dong LC, Hoffman AS, Yan Q, Dextran permeation through poly(N-isopropylacrylamide) Hydrogels, J. Biomater. Sci. Polym. Ed 5 (1994) 473–484. doi: 10.1163/156856294X00158. [PubMed: 7518690]

[67]. Hoffman AS, Hydrogels for biomedical applications, Adv. Drug Deliv. Rev 64 (2012) 18–23. doi: 10.1016/j.addr.2012.09.010.

[68]. Wang HB, Dembo M, Wang YL, Substrate flexibility regulates growth and apoptosis of normal but not transformed cells., Am. J. Physiol. Cell Physiol 279 (2000) C1345–C1350. doi: 11029281. [PubMed: 11029281]

[69]. Flory PJ, Molecular size distribution in three dimensional polymers, J. Am. Chem. Soc 63 (1941) 3083–3100. doi:10.1021/ja01856a061.

[70]. Stockmayer WH, Theory of molecular size distribution and gel formation in branched polymers: II. General cross linking, J. Chem. Phys 12 (1944) 125–131. doi: 10.1063/1.1723922.

[71]. Tevis KM, Colson YL, Grinstaff MW, Embedded Spheroids as Models of the Cancer Microenvironment, Adv. Biosyst 1700083 (2017) 1700083. doi:10.1002/adbi.201700083.

[72]. Cheng G, Tse J, Jain RK, Munn LL, Micro-Environmental Mechanical Stress Controls Tumor Spheroid Size and Morphology by Suppressing Proliferation and Inducing Apoptosis in Cancer Cells, PLoS One. 4 (2009) e4632. doi: 10.1371/journal.pone.0004632. [PubMed: 19247489]

[73]. Helmlinger G, Netti PA, Lichtenbeld HC, Melder RJ, Jain RK, Solid stress inhibits the growth of multicellular tumor spheroids, Nat. Biotechnol 15 (1997) 778–783. doi: 10.1038/nbt0897-778. [PubMed: 9255794]

[74]. Chen CS, Mrksich M, Huang S, Whitesides GM, Ingber DE, Geometric control of cell life and death., Science. 276 (1997) 1425–1428. doi:10.1126/science.276.5317.1425. [PubMed: 9162012]

[75]. Leight JL, a Wozniak M, Chen S, Lynch ML, Chen CS, Matrix rigidity regulates a switch between TGF-β1-induced apoptosis and epithelial-mesenchymal transition., Mol. Biol. Cell 23 (2012) 781–91. doi:10.1091/mbc.Ell-06-0537. [PubMed: 22238361]

[76]. Dupont S, Morsut L, Aragona M, Enzo E, Giulitti S, Cordenonsi M, Zanconato F, Le Digabel J, Forcato M, Bicciato S, Elvassore N, Piccolo S, Role of YAP/TAZ in mechanotransduction., Nature. 474 (2011) 179–183. doi:10.1038/naturel0137. [PubMed: 21654799]

[77]. Aragona M, Panciera T, Manfrin A, Giulitti S, Michielin F, Elvassore N, Dupont S, Piccolo S, A mechanical checkpoint controls multicellular growth through YAP/TAZ regulation by actin-processing factors, Cell. 154 (2013) 1047–1059. doi: 10.1016/j.cell.2013.07.042. [PubMed: 23954413]

[78]. Pinter M, Jain RK, Targeting the renin-angiotensin system to improve cancer treatment: Implications for immunotherapy, Sci. Transl. Med 9 (2017). doi: 10.1126/scitranslmed.aan5616.

[79]. Grinstaff MW, Kaplan H, Kohn J, Predoctoral and Postdoctoral Training Pipeline in Translational Biomaterials Research and Regenerative Medicine, ACS Biomater. Sci. {&} Eng (2017) acsbiomaterials.7b00268. doi:10.1021/acsbiomaterials.7b00268.

Statement of Significance:

In this study, we have developed, optimized, and applied a novel 3D *in vitro* cell culture platform composed of an interpenetrating network (IPN) that is both mechanically tunable and inherently bioactive. The IPN consists of a primary fibrillar collagen type-1 network reinforced by a secondary thiol-ene poly(ethylene glycol) (PEG) network. The IPNs are formed via a novel strategy in which cell-laden collagen gels are formed first, and soluble PEG monomers are added later and crosslinked via visible light. This approach ensures that the collagen gels contain a fibrillar architecture similar to the collagen architecture present *in vivo.* We applied our IPN platform to study the effect of mechanical confinement on cancer cell behavior and found that it inhibits malignant-like behavior.

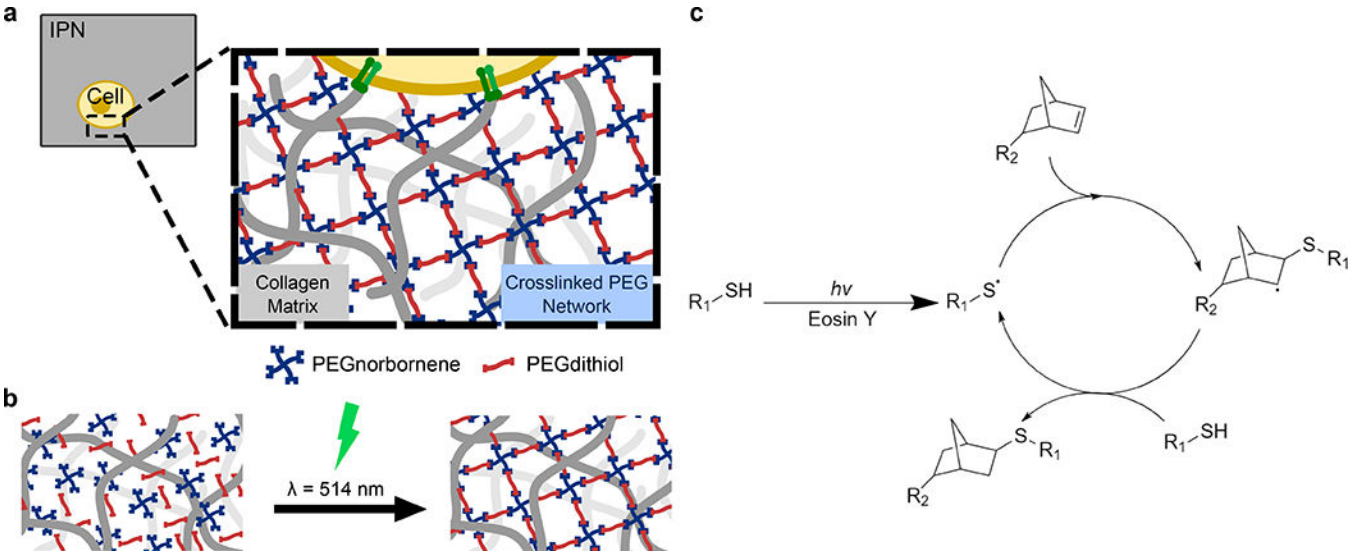

Figure 1: Overview of PEG/Collagen Interpenetrating Network.

a) Overview of PEG/Collagen IPN. b) Soluble PEG monomers are delivered to 3D collagen networks and crosslinked *in situ* using visible light. c) Schematic of visible light-mediated thiol-ene photopolymerization using Eosin Y as the photoinitiator.

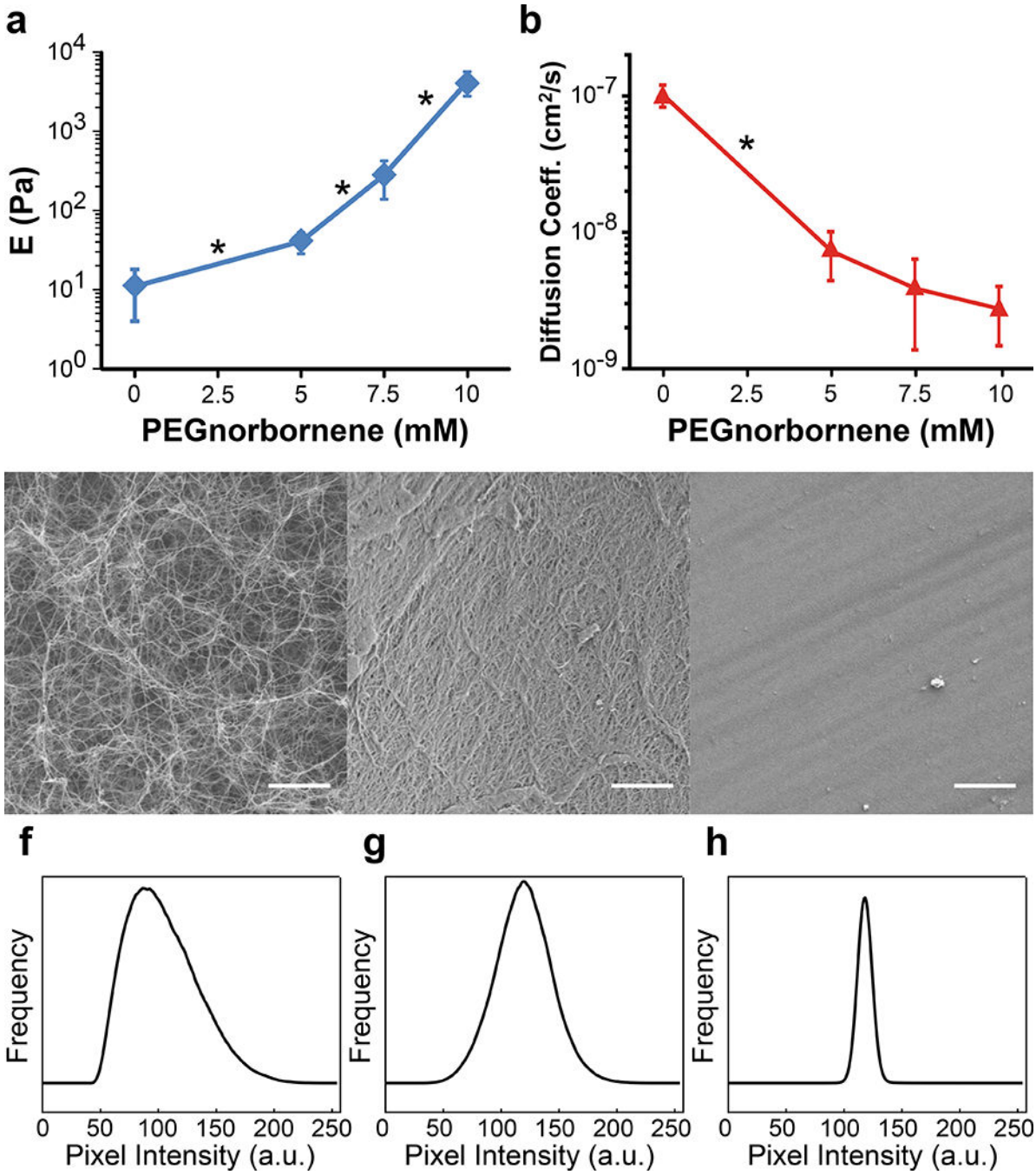

Figure 2: Material Characterization of PEG/Collagen IPNs.

a) Mechanical testing revealed the elastic moduli of PEG/Collagen IPNs spans several orders of magnitude from ~10 Pa to ~4 kPa. b) The diffusion coefficients of BSA-AlexaFluor 594 within PEG/Collagen IPNs, as calculated by the semi-infinite slab approximation, demonstrates that the secondary PEG network hinders biomolecular transport. The microstructures of the IPN system were investigated using SEM imaging, and representative images of the c) collagen-only, d) PEG/Collagen IPN with 10 mM PEG4NB, and e) PEG-only gels with 10 mM PEG4NB are shown. Histogram of pixel intensity for f) collagen-only,

g) PEG/Collagen IPN, and h) PEG-only gels is also shown. The left-shifted curve in the histogram for the pure collagen condition reflects its highly porous microstructure, while the more normalized curve in the PEG/collagen IPN histogram is indicative of the secondary PEG network interpenetrating the porous collagen network. Data presented as mean ± SD; n = 3. P value determined using ANOVA with Tukey-Kramer post hoc analysis (*$P < 0.001$).

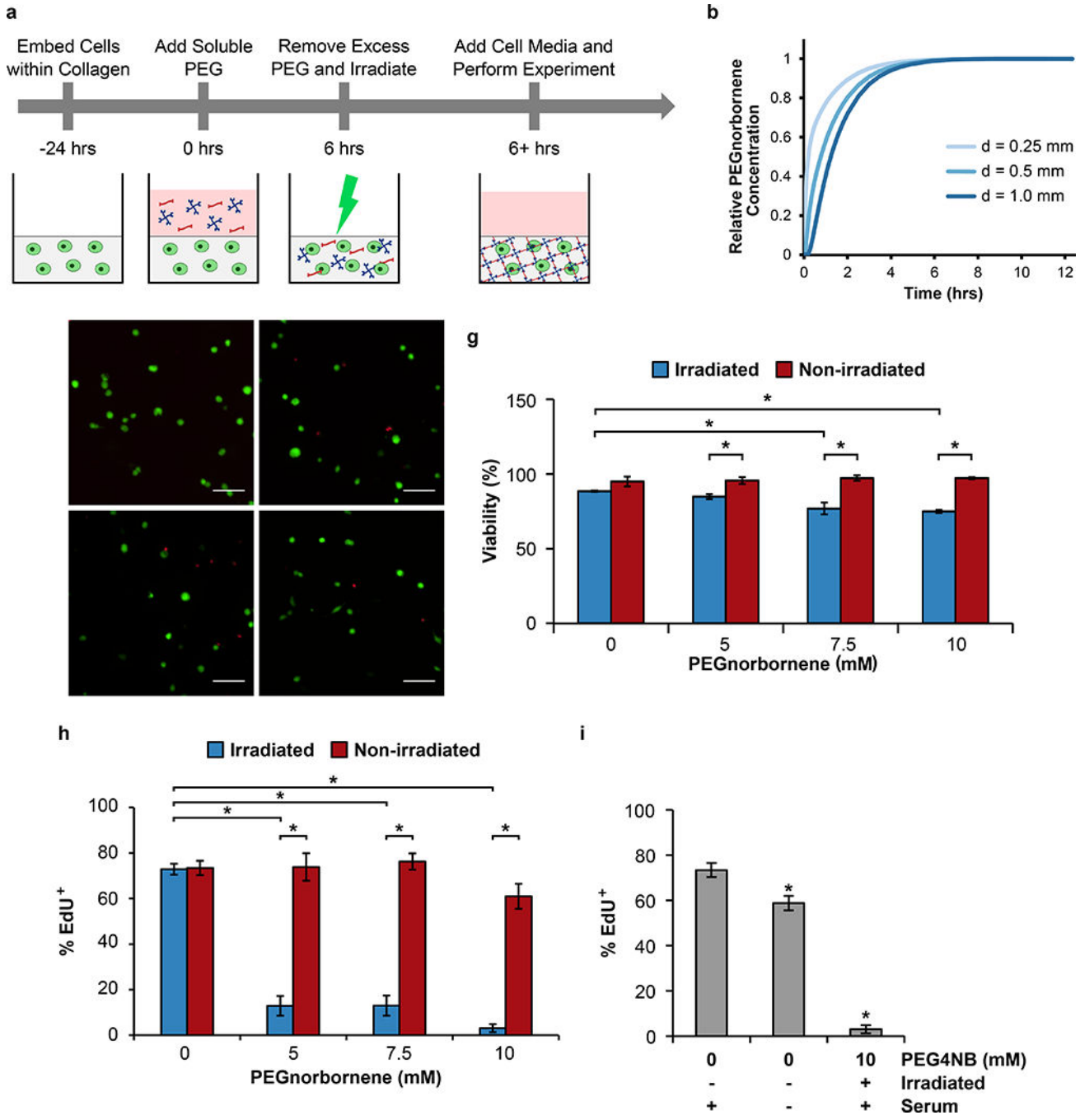

Figure 3: Cellular Response to PEG/Collagen IPNs.

a) The experimental work flow for generating PEG/Collagen IPNs is shown and consists of the following: 1) embedding cells within 3D collagen gels 24 hours prior to adding the soluble polymer solution, 2) adding the soluble polymer solution and allowing 6 hours for the polymer to fully diffuse into the collagen gel, 3) removing excess polymer solution and irradiating the sample with visible light to initiate crosslinking, 4) washing the sample 3x's with cell culture media to remove any uncrosslinked monomers, and 5) adding a final volume of cell culture media to the IPN and proceeding to perform the experiment of

interest, b) Mathematical modeling of PEG4NB diffusion predicts our system reaches diffusive equilibrium within 6 hours. LIVE/DEAD staining for MDA.MB.231 cells embedded within PEG/Collagen IPNs containing c) 0 mM, d) 5 mM, e) 7.5 mM, and f) 10 mM PEG4NB. g) Viability analysis of LIVE/DEAD images showed a slight, but significant, decrease in viability for the irradiated PEG/Collagen IPN conditions (blue), but not in the non- irradiated controls (red). h) Proliferation analysis of MDA.MB.231 cells within PEG/Collagen IPNs revealed a significant decrease in proliferation for the irradiated PEG/Collagen IPN conditions (blue), but not in the non-irradiated controls (red). i) Serum-starvation had a slight effect on proliferation, but not to the same degree as cells embedded within the PEG/Collagen IPN condition. Data presented as mean ± SD; n = 3 gels, 4 locations per gel. P value determined using ANOVA with Tukey-Kramer post hoc analysis (*$P < 0.05$).

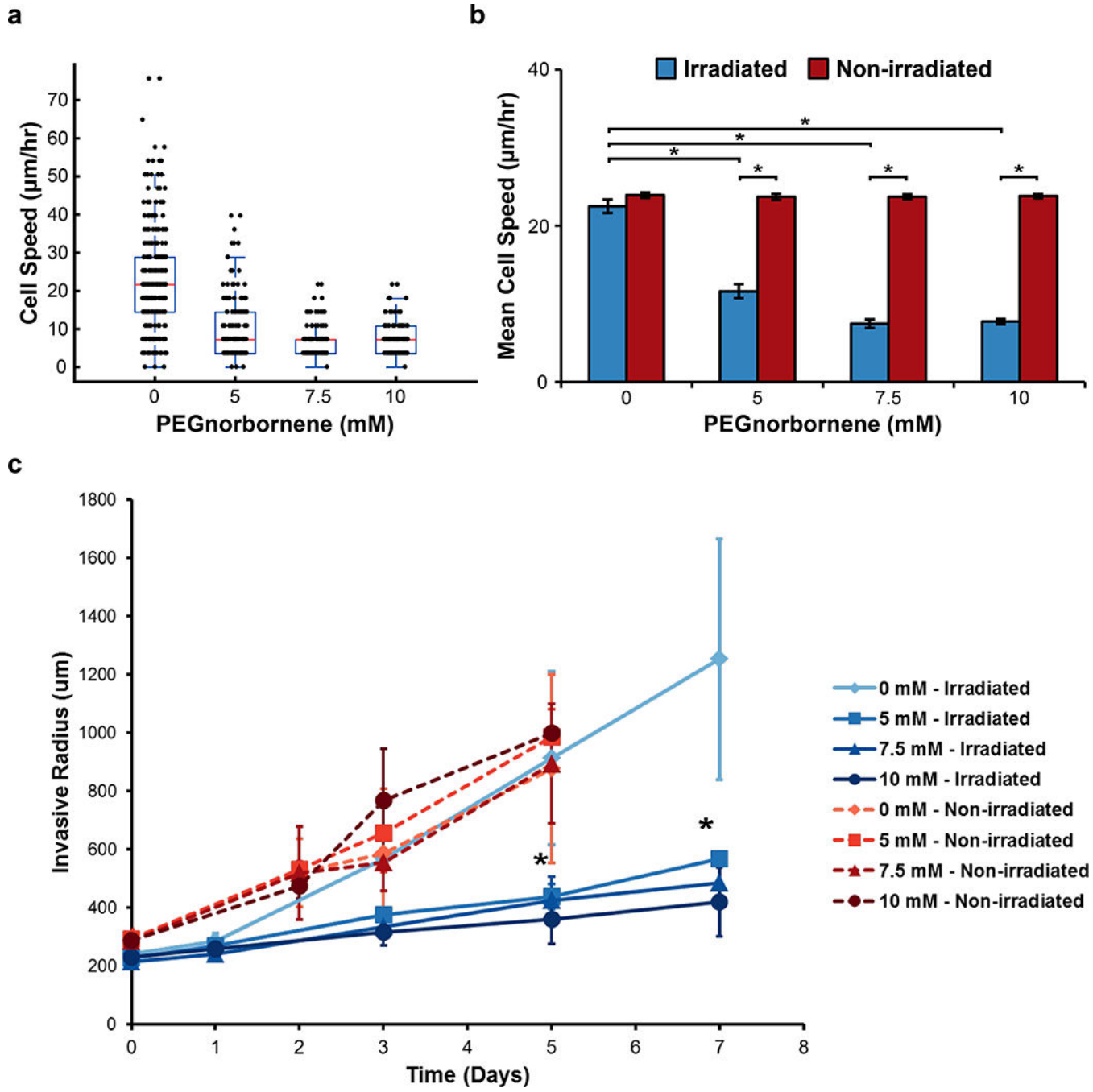

Figure 4: Analysis of Cell Motility within PEG/Collagen IPNs.

a) Box-whisker plot of migration speed of individual MDA.MB.231 cells embedded diffusely within PEG/Collagen IPNs over the course of 24 hours immediately following crosslinking. b) The average cell speed for the entire population of cells within the irradiated PEG/Collagen IPNs or non-irradiated controls (mean ± SEM; n = 3 gels, 2 locations per gel). P value determined using ANOVA with Tukey-Kramer post hoc analysis (*P < 0.001).

c) The average invasive radius of MDA.MB.231 multicellular spheroids embedded within PEG/Collagen IPNs were measured as a function of time (mean ± SEM; n = 3 spheroids).